ELSEVIER

NeuroImage

www.elsevier.com/locate/ynimg
NeuroImage 35 (2007) 89–104

Depth-resolved optical imaging and microscopy of vascular compartment dynamics during somatosensory stimulation

Elizabeth M.C. Hillman,[a,*] Anna Devor,[a,b] Matthew B. Bouchard,[a] Andrew K. Dunn,[c] G.W. Krauss,[a] Jesse Skoch,[d] Brian J. Bacskai,[d] Anders M. Dale,[b] and David A. Boas[a]

[a]*Athinoula A. Martinos Center for Biomedical Imaging, Massachusetts General Hospital, Building 149, 13th Street, Charlestown, MA 02129, USA*
[b]*Neuroscience and Radiology, University of California San Diego, 9500 Gillman Drive, La Jolla, CA 92093, USA*
[c]*Biomedical Engineering, University of Texas at Austin, 1 University Station, C0800, Austin, TX 78712, USA*
[d]*Neurology, Massachusetts General Hospital, Building 114, 16th Street, Charlestown, MA 02129, USA*

Received 11 August 2006; revised 26 October 2006; accepted 17 November 2006
Available online 11 January 2007

The cortical hemodynamic response to somatosensory stimulus is investigated at the level of individual vascular compartments using both depth-resolved optical imaging and in-vivo two-photon microscopy. We utilize a new imaging and spatiotemporal analysis approach that exploits the different characteristic dynamics of responding arteries, arterioles, capillaries and veins to isolate their three-dimensional spatial extent within the cortex. This spatial delineation is validated using vascular casts. Temporal delineation is supported by in-vivo two-photon microscopy of the temporal dynamics and vascular mechanisms of the arteriolar and venous responses.

Using these techniques we have been able to characterize the roles of the different vascular compartments in generating and controlling the hemodynamic response to somatosensory stimulus. We find that changes in arteriolar total hemoglobin concentration agree well with arteriolar dilation dynamics, which in turn correspond closely with changes in venous blood flow. For 4-s stimuli, we see only small changes in venous hemoglobin concentration, and do not detect measurable dilation or ballooning in the veins. Instead, we see significant evidence of capillary hyperemia.

We compare our findings to historical observations of the composite hemodynamic response from other modalities including functional magnetic resonance imaging. Implications of our results are discussed with respect to mathematical models of cortical hemodynamics, and to current theories on the mechanisms underlying neurovascular coupling. We also conclude that our spatiotemporal analysis approach is capable of isolating and localizing signals from the capillary bed local to neuronal activation, and holds promise for improving the specificity of other hemodynamic imaging modalities.

Introduction

The cortical hemodynamic response to stimulus provides a detectable signal which can report the presence and location of neuronal activation (Fox and Raichle, 1986; Woolsey et al., 1996). Functional Magnetic Resonance imaging (fMRI) provides an unsurpassed tool with which to image the hemodynamic response non-invasively and in a clinical setting (Belliveau et al., 1991). However, interpretation of fMRI data is confounded by relatively poor specificity to neuronal events: The MRI-based blood oxygen level dependent (BOLD) signal is primarily sensitive to deoxy-hemoglobin concentration changes, and originates in both the capillary beds of the cortex as well as in more distant draining veins (Mandeville et al., 1999; Turner, 2002).

Consensus has also yet to be reached about the neurovascular mechanisms by which the cortical hemodynamic response arises, both in terms of how it is triggered and controlled, and how it proceeds as the stimulus response evolves (Attwell and Iadecola, 2002; Iadecola, 2004). To date, the hemodynamic response has largely just been considered as the sum total of all the activity observed that temporally correlates with a presented stimulus (Arthurs and Boniface, 2002; Iadecola, 2002). In this paper we utilize the well characterized rat forepaw stimulus model and apply novel optical imaging technologies to investigate the hemodynamic response in detail. Using high resolution optical imaging and microscopy, we are able to resolve the behavior of the individual vascular compartments involved in the ensemble hemodynamic response. By investigating the role of each compartment, we are able to more fully understand both the composition, and basic mechanisms of the observable hemodynamic signal.

Optical imaging of the exposed cortex not only provides high spatial resolution, but also high frame rates and simultaneous sensitivity to oxy-, deoxy- and total hemoglobin changes (HbO_2, HbR and HbT) (Devor et al., 2003; Hewson-Stoate et al., 2005; Malonek and Grinvald, 1996; Sheth et al., 2005). However,

* Corresponding author. 351L Engineering Terrace, Department of Biomedical Engineering, Columbia University, 1210 Amsterdam Avenue, New York, NY 10027, USA. Fax: +1 212 854 8725.
E-mail address: eh2245@columbia.edu (E.M.C. Hillman).
Available online on ScienceDirect (www.sciencedirect.com).

1053-8119/$ - see front matter © 2006 Elsevier Inc. All rights reserved.
doi:10.1016/j.neuroimage.2006.11.032

camera-based optical imaging only provides 2-dimensional (2D) images of the cortical surface, making it difficult to quantify and distinguish between signals from superficial vasculature and deeper capillary beds. In this paper, we utilize a recently developed optical imaging technology called Laminar Optical Tomography (LOT) (Hillman et al., 2004), which is capable of high-resolution depth-resolved imaging of hemodynamic activity in the cortex to depths of around 2 mm. We complement LOT with rapid, full-field two photon microscopy, both to validate our LOT findings, and to further explore the vascular mechanisms of the hemodynamic response in-vivo.

Using LOT, we demonstrate that it is possible to distinguish subtle yet distinctive functional temporal signatures associated with the hemodynamic response in the different vascular compartments. We show that these signatures can be used to *spatially* resolve the locations of the different compartments in the cortex in 3-dimensions (3D). We validate our findings with two-photon microscopy of vascular casts from the same rats. We further demonstrate that these differences in the vascular compartment responses are robust, and have potential as a mechanism for spatiotemporal separation of the vascular compartments in other functional imaging modalities including fMRI.

The extracted temporal signatures of the vascular compartments also provide new insights into the vascular mechanisms taking place. We utilize in-vivo two-photon microscopy of vessels in the brain during somatosensory stimulus to further validate and explore the physical vascular mechanisms that underlie the distinct temporal characteristics of the functional response in each compartment.

We present evidence that arteriolar dilation dynamics correlate strongly with the blood flow response in the veins. We further show that, for 4 s stimuli, the most significant changes in the venous compartment are speed of flow and oxygenation changes, and not venous dilation or ballooning. We utilize our results to revisit standing theories and assumptions about neurovascular coupling and how the hemodynamic response is controlled, including capillary hyperemia and directional propagation of vasodilation. We discuss the implications of our findings to hemodynamic modeling and to other functional imaging modalities.

Methods

In-vivo imaging experiments were performed using rats undergoing 4-s-long electrical forepaw stimulation (Brecht et al., 2003; Jones et al., 2001; Mandeville et al., 1999; Pain et al., 2002; Sheth et al., 2005; Shibuki et al., 2003; Silva and Koretsky, 2002). Detailed procedures are described below.

Animal preparation

Sprague–Dawley rats (310 g±40 g) were prepared under isoflurane anesthesia (1–3% in 25% Oxygen, 75% air). After placement of a tracheotomy and femoral arterial and venous catheters, the head was fixed in a stereotaxic frame, the scalp was retracted, and a ~5 mm×5 mm area of skull over the somatosensory cortex was thinned to translucency. Where two-photon microscopy was performed (10 rats); the IVth ventricle was opened to relieve intra-cerebral pressure, and the thinned skull area was removed along with the dura. 1.5% agarose (Fluka) in artificial cerebrospinal fluid (Kleinfeld and Delaney, 1996) was placed onto the exposed cortex and covered with a small glass coverslip. The window was then sealed relative to the skull with dental acrylic to minimize brain motion and contamination. For LOT imaging (8 rats), the thinned skull was kept intact.

Following surgery, isoflurane was discontinued, and replaced with intravenous delivery of alpha-chloralose (30–40 mg/kg/h). Throughout data collection, the animals were mechanically ventilated with a 3:1 ratio of air and oxygen, and systemic blood pressure and depth of anesthesia were monitored and maintained within normal ranges (pressure: 100 mm Hg±20 mm Hg, anesthesia level: below threshold of hind-paw withdrawal, maintained via slight adjustments to anesthesia and ventilation parameters). Blood gas values were measured when necessary to ensure good systemic physiology.

Electrodes placed on the right forepaw were connected to an electrical stimulus isolation unit (WPI Inc, Sarasota, Florida, USA) delivering 3 μs pulses at 3 Hz with 1.6 mA±0.6 mA amplitude (each animal's stimulus amplitude was adjusted to just below movement threshold). The stimulus block consisted of 3 s blank followed by 4 s of stimulus and then 20 s of blank again before the next block. All animal procedures were reviewed and approved by the Subcommittee on Research Animal Care at Massachusetts General Hospital, where these experiments were performed.

2D optical imaging of exposed cortex

In all experiments, the rats were first imaged using conventional 2D optical imaging to verify the location of the response area and to confirm the physiological stability of the animal. 30 repetitions of the forepaw stimulus were presented while the cortex was illuminated with 570 nm light and imaged using a CCD camera (~8 frames per second). The resulting data were block-averaged and maps and timecourses of the % signal change during stimulus (proportional to HbT change) were examined. Where necessary, physiological parameters were assessed and adjusted, and the measurement repeated until a normal response was observed (defined as a cleanly rising and falling HbT response with a stable baseline and with a $\Delta R/R$ amplitude between 0.5% and 3%).

3D Laminar Optical Tomography (LOT)

LOT was developed to provide depth-resolved optical imaging of living tissues (Dunn and Boas, 2000; Hillman et al., 2004) and combines the principles of laser scanning confocal microscopy with scattered-light tomography reconstruction techniques. LOT can provide imaging to depths of >2 mm with 100–200 μm resolution (dependent on the type of tissue being imaged, and with lower resolution at deeper depths). This depth sensitivity exceeds the scattering limits faced by conventional microscopy, and LOT is also highly sensitive to absorption, and therefore hemoglobin concentration changes.

A schematic of the LOT system is shown in Fig. 1A. LOT has been validated using tissue-simulating phantoms as described in (Hillman et al., 2004). In this paper, we utilize an upgraded system for in-vivo hemodynamic imaging. The new system utilizes multi-wavelength scanning (473 nm and 532 nm) and acquires up to 10 3D image frames per second.

The LOT system is similar to a low magnification scanning confocal microscope, but rather than scanning its focus in the *z*-direction, LOT instead measures both the confocal and the scattered reflected light to probe sub-surface absorption. Scattered

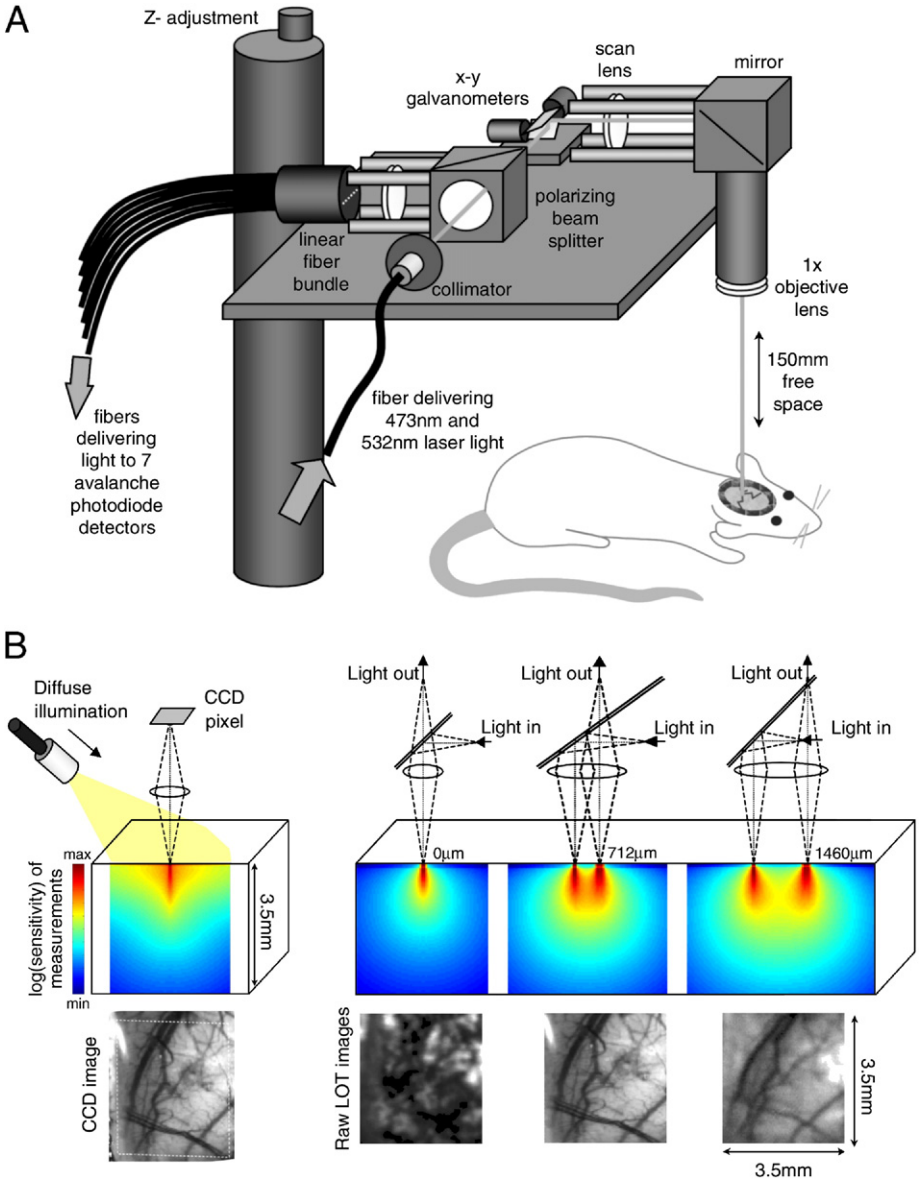

Fig. 1. Laminar optical tomography. (A) LOT system for depth-resolved hemodynamic imaging of rat cortex. (B) (Upper left) spatial measurement sensitivity profile of a single CCD image pixel with oblique illumination, (lower left) corresponding image of rat cortex through thinned skull at 570 nm, (upper right) spatial sensitivity profile of LOT measurement geometries where illumination and detection are gradually offset from one another. (Lower right) corresponding raw LOT images of the same cortical region in the same rat (at 532 nm). As predicted by the sensitivity profiles, the geometry with 0 mm separation between illumination and detection is sensitive mostly to the superficial layers of the thinned skull. The wider source-detector separations (712 um and 1460 um) provide gradually increasing depth sensitivity.

light is detected from 7 positions adjacent to the scanning laser beam's focus (between 0 and 2 mm away). The further from the focus that the scattered light emerges, the deeper on average it has traveled into the cortex, and can therefore be used to distinguish between events happening in superficial versus deeper tissue. The spatial sensitivity profiles of each measurement can be simulated using Monte-Carlo modeling of light propagation (Dunn and Boas, 2000). Representative examples of these profiles are shown in Fig. 1B.

As the focused beam is raster scanned over the surface of the thinned skull, light detected simultaneously from the 7 offset positions forms 7 'raw' images of the cortex, each with a different measurement depth-sensitivity. Each *raw* LOT image represents a different combination of signals from different depths: e.g. in Fig. 1B, the 0 μm offset raw image predominantly reveals the rough surface of the thinned skull, whereas measurements with wider offsets accentuate the underlying blood vessels and the parenchyma.

However, these raw images are not true depth-sections. In order to convert these images into a proper 3D rendering, the simulated depth-sensitivity profiles for each measurement are combined with the raw data using a computed-tomography-like deconvolution procedure (Dunn and Boas, 2000; Hillman et al., 2004). The resulting 3D images of the absorption changes corresponding to each wavelength can then be converted into quantitative mM maps of oxy-, deoxy- and total hemoglobin changes (ΔHbO_2 and ΔHbR and $\Delta HbT = \Delta HbO_2 + \Delta HbR$) via the spectra of HbO_2 and HbR

(Hillman, 2002). This reconstruction procedure is similar to that used in diffuse optical tomography of large tissue volumes (Arridge, 1999) although much higher resolution is attained (100–200 μm), and modeling must carefully account for sub-millimeter length scales of LOT. While the LOT reconstruction process is dependent on an initial model of light propagation, it intrinsically compensates for optical pathlength effects by modeling the way that light scatters differently at the two measurement wavelengths.

In eight rats, the LOT system was used to acquire series of 90 images, at each interleaved wavelength, during the first 23 s of each stimulus block. Between 140 and 500 separate stimulus blocks were recorded for each rat. Exclusion criteria were applied to eliminate data corresponding to poor systemic physiology (unstable blood pressure or heart rate), bruising of the brain or movement artifacts. The remaining scans for each rat were then co-registered and calibrated via measurements of 'dark' signals, and the block-averaged percentage changes relative to pre-stimulus baseline were calculated. Dual wavelength data were temporally interpolated onto the same time-base, and then converted into 3D images of hemoglobin concentration changes as described above. Additional details about LOT data and image processing methods are provided in the supplementary data.

Resin casts of cortical vasculature

Following LOT imaging, euthanasia and flushing with phosphate-buffered saline, the carotid arteries of each rat were injected with a mixture of Batsons #17 corrosion casting resin, Methyl-methacrylate and a small amount of rhodamine B in Dimethylsulfoxide (DMSO) (Harrison et al., 2002; Rodriguez-Baeza et al., 1998). Following refrigeration and excision of the brain, some samples were preserved in formalin, while others were placed in a KOH solution at 50 °C to macerate the soft tissue. The addition of rhodamine to the resin allowed ex-vivo depth-resolved imaging of the vascular architecture using a commercial Radiance 2000 Biorad two-photon microscopy system.

In-vivo two-photon microscopy of functional activity

We recently constructed an in-vivo two-photon microscopy system, specifically designed to allow very rapid, whole-field imaging of vascular hemodynamics in-vivo (Bouchard et al., 2006). The system, based on a tunable Ti:Sapphire laser (Mai-Tai, Spectra Physics) is able to image at up to 22 frames per second. Such systems have been shown to be capable of in-vivo imaging of the dynamics of blood flow in addition to neuronal activity via calcium sensitive dyes (Hutchinson et al., 2006; Kleinfeld et al., 1998; Ohki et al., 2005).

Following surgery as described above, rats first underwent 2D CCD-based imaging to localize the region of the somatosensory cortex activated by forepaw stimulus. The rats were then transferred to a motorized *x–y* stage positioned under the microscope's objective (Olympus XLUMPlanFl 20x/0.95W). The forepaw response region was identified by visually inspecting the vasculature and comparing to the CCD images. Dextran-conjugated fluorescein (FD2000S, Sigma-Aldrich, 10 mg in 0.2 ml saline) was then injected intravenously and images were acquired at 800 nm two-photon excitation.

Once a suitable network of vessels was positioned in the field of view, in-plane two-photon images were acquired at 14 frames per second for 20 s during a 4 s forepaw stimulus block (with the same stimulus parameters as for LOT experiments). Images show the fluorescein in the blood plasma, making it possible to observe the dynamics of the vessel walls as well as the red blood cells (RBCs, which appear as shadows) (Kleinfeld et al., 1998; Villringer et al., 1994). By imaging whole fields-of-view rather than just line scans, we are able to observe dynamics in multiple vessels and compartments simultaneously, and extract their blood flow flux, speed, RBC density and vessel diameter variations in response to each individual stimulus.

Results

Depth-resolved imaging of the hemodynamic response

Fig. 2 shows depth-resolved cortical functional activation maps from one rat, acquired using LOT during electrical forepaw stimulation; Fig. 2A shows a CCD camera image of the field of view, acquired with 570 nm illumination prior to LOT imaging (the LOT field of view is identified by the dotted white square). Fig. 2B shows horizontal LOT slices of the depth-resolved HbR, HbO_2 and HbT functional changes 0.6 s after cessation of the stimulus (block-average of 140 stimuli). The most superficial (0 μm) slice partially samples the dura and cerebrospinal fluid and the very top of the superficial vasculature. The 200 μm depth slice shows more of the pial vasculature, and contains some signal from the superficial cortex (layer I). The 600 μm deep slice corresponds to deeper cortical layers (layers III–IV) and predominantly reveals changes in the capillary bed.

Figs. 2C and D show vertical slices through the 3D HbO_2 data in the *x–z* plane. The vertical slice locations are labeled i and ii in A and B, and transect a surface draining vein and the focal capillary region respectively. The depth-resolved time courses of HbO_2, HbR and HbT in these regions (along the dotted vertical lines) are also shown.

Fig. 2C illustrates the superficial location of the draining vein. The depth-resolved time-courses for this slice show little change in the cortex below the vein. It is also interesting to note that the vein does not appear to exhibit significant HbT changes. In contrast, Fig. 2D shows a much deeper response, corresponding to a combination of capillary bed activation and diving arterioles and venules, in addition to superficial signals from the pial vasculature. Timecourses from the layers in this slice reveal changes in HbO_2, HbR and HbT to depths of >1400 μm. Equivalent results for a second rat are shown in the supplementary data (Fig. S1).

Spatiotemporal isolation of vascular compartments

While the 3D LOT images of the vasculature can spatially resolve structures corresponding to superficial vessels and deeper capillary beds, we wish to exploit this spatial separation to examine the dynamic behavior of each vascular compartment individually.

We can readily extract the HbR, HbO_2 and HbT timecourses of the voxels corresponding only to the superficial draining vein (labeled 'v' in Fig. 2B), and similarly for the deeper capillary bed region (region 'c'). In addition, we notice that there is a 3rd distinct region, visible in the 200 μm deep HbT image. This region does not seem to exhibit a substantial HbR change, and is superficial. From comparison with the grayscale CCD images, we conclude that this region is a surface arteriole (region 'a' in Fig 2B). The functional timecourses from these three regions are shown in Fig.

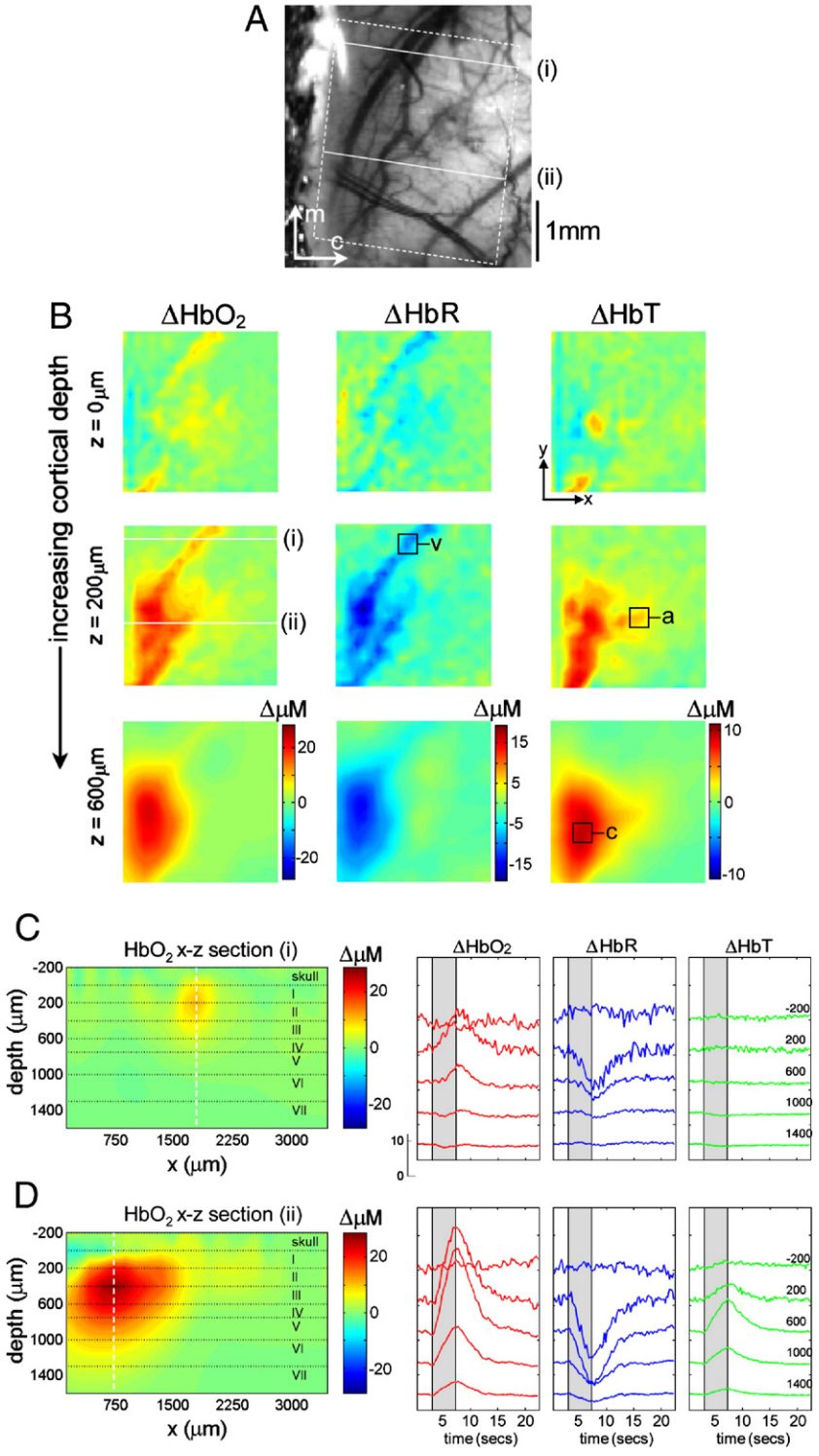

Fig. 2. Depth-resolved hemodynamic imaging. (A) CCD image of rat cortical surface through thinned skull. The region imaged using LOT is indicated by the white dotted lines. (B) Depth-resolved LOT images of oxy-, deoxy- and total hemoglobin concentration changes in the cortex 0.6 s after cessation of a 4 s forepaw stimulus at cortical depths of 0, 200 and 600 μm. (C) Depth-resolved cross section of the HbO_2 response at the position indicated with (i) in panel B, representing a large draining vein. The corresponding HbO_2, HbR and HbT depth-resolved time-courses around $x = 1800$ μm (dotted white line) are shown to the right. (D) Depth-resolved cross section of the HbO_2 response at the position indicated with (ii) in panel B. The corresponding HbO_2, HbR and HbT depth-resolved time-courses around $x = 750$ μm are shown to the right. Numbers on each temporal trace represent their depth of origin in microns. 'a', 'v' and 'c' denote regions identified as arteriole, vein and capillary for timecourse extraction.

3A, normalized to the peak of their HbO_2 response. The mean averages of similarly selected regions from 5 rats are shown in Fig. 3B (error bounds show the standard error on the mean).

There are many statistically significant differences between the evolution of HbR, HbO_2 and HbT across these vascular compartments which are consistent across all 5 rats (as described in more detail below). Strong features include: 1) The delay in venous HbO_2 and HbR responses relative to the arteriolar and capillary compartments, 2) the small magnitude of the venous HbT change, 3) the rapid onset and decay of the arteriolar response, and 4) the latency of the capillary post-stimulus decay. These observations are consistent with the compartment-specific onset hemodynamics in the superficial cortical vasculature of cats as reported by (Vanzetta et al., 2005), and in rat somatosensory cortex as reported by (Li et al., 2003; Sheth et al., 2005) using 2D optical imaging. Berwick et al. (2005) and Vanzetta et al. (2005) also note small venous HbT changes.

To ensure that these timecourse differences are not the result of subjective selection of voxels, the process was repeated using only a simple algorithm which sought regions with common functional behavior (looking for major features such as delayed HbO_2 onset, prompt decay and high amplitude changes in HbO_2, HbT and HbR). The result was a set of masks which corresponded to the voxels exhibiting this behavior, and which overlaid well with the regions selected subjectively The functional timecourses extracted using these masks were almost identical to those shown in Figs. 3A and B. (These masks are shown for two rats in supplemental data, Fig. S3.)

The extracted compartment timecourses are distinct signatures of each vascular compartment, a result of differing structural and physical properties such as smooth muscle, compliance and oxygen perfusability. Based on this, we hypothesized that each voxel in our 3D time-series of HbR, HbO_2 and HbT could be represented purely as a linear combination of arteriole, capillary and vein, e.g:

$$\begin{bmatrix} I_{\mathrm{HbO}}(r,t) \\ I_{\mathrm{Hb}}(r,t) \\ I_{\mathrm{HbT}}(r,t) \end{bmatrix} = \begin{bmatrix} c_{\mathrm{HbO,\ artle}}(t) & c_{\mathrm{HbO,\ vein}}(t) & c_{\mathrm{HbO,\ cap}}(t) \\ c_{\mathrm{Hb,artle}}(t) & c_{\mathrm{Hb,vein}}(t) & c_{\mathrm{Hb,cap}}(t) \\ c_{\mathrm{HbT,\ artle}}(t) & c_{\mathrm{HbT,\ vein}}(t) & c_{\mathrm{HbT,cap}}(t) \end{bmatrix} \begin{bmatrix} I_{\mathrm{artle}}(r) \\ I_{\mathrm{vein}}(r) \\ I_{\mathrm{cap}}(r) \end{bmatrix} \quad (1)$$

where $c(t)$ is a compartment's functional time-course, $I_{\mathrm{HbO}}(r,t)$ is the 3D HbO_2 image series, and $I_{\mathrm{artle}}(r)$ is an image of the arteriolar component ($I_{\mathrm{cap}}(r)$ is capillary and $I_{\mathrm{vein}}(r)$ is venous).

If we solve Eq. (1) for $I_{\mathrm{compartments}}$ using a non-negative least-square fit (Lawson and Hanson, 1974), the result will be 3D images of the three vascular compartments involved in the functional response, based only on their characteristic temporal HbR, HbO_2 and HbT dynamics. The results of this spatiotemporal separation are shown in Fig. 3C, where each column shows image slices at different depths (compare to Fig. 2B). Each image depicts regions whose functional time-courses correlate with the dynamic behavior of arterioles, capillaries and veins (from left to right).

Note the accentuation of confluent, vessel-like structures in the arteriolar and venous images, and the deeper rounded shape of the capillary compartment. These three components are also shown as 3D surface renderings (40% isosurfaces) in Fig. 3D. Equivalent results for a second rat are shown in the supplementary data (Fig. S2). A similar compartment-resolved result for 2D optical imaging was recently obtained with an automated spatiotemporal separation algorithm (Berwick et al., 2005).

The residuals of our spatiotemporal fit are small, suggesting that much of the vasculature within a compartment indeed reacts with very similar characteristic timecourses as those shown. As detailed in supplementary data (Fig. S4): only one region was found to be unaccounted for in this spatiotemporal fit. This region exhibited a response with negligible HbR change. When the functional timecourse of this region was incorporated into a 4 component fit, the response localized to the base of the large artery, and the residuals of the 4 component fit were uniformly small. The lack of HbR response in the main artery is consistent with a high (~98%) baseline oxygen saturation. Quantification of the residuals and singular value decomposition of the data also confirms that the main compartment timecourses are highly representative of the first three orthogonal components of the entire data set, accounting for ~85% of the total variance (see Fig. S4). We expect that the remaining variance accounts for the behaviors of transition vessels such as pre- and post-capillary arterioles and venules, as well as local subtleties of the temporal responses.

Spatial validation: comparison of compartments with 3D vascular architecture

Although the structures isolated from their dynamic behavior resemble confluent vessels, we can in fact validate whether these regions correspond to the correct vascular architecture using the ex-vivo vascular casts created following LOT data acquisition. Fig. 3F shows a two-photon image stack of the (un-macerated) ex-vivo vascular cast of the same animal. Identification of arterial, arteriolar and venous vasculature is based on vessel smoothness, direction and connectivity. In Fig. 3E, the superficial vascular patterns from the cast have been overlaid on the 200 μm deep (pial-to-layer I) LOT slice. The capillary region identified by LOT is overlaid in green onto the vascular cast image.

These results illustrate the strong agreement between the regions identified by their dynamics using LOT and the physical vasculature from the vascular casts, particularly for the venous compartment. For the arteriolar compartment the match to the static vessels is not exact, however this illustrates an important and useful facet of this method: Since the maps reveal regions responding with a characteristic timecourse, only those branches of the arteriolar tree that are recruited during the functional response are visible in the LOT result. The broader arterial base also does not appear owing to its differing functional response as shown in Supplemental figure S4.

We can also compare the *depth-resolved* compartment structures with the static vascular architecture. For the rats whose vascular casts were placed in KOH to macerate away soft tissue, only a very fine structure of vessels remained which could be imaged using two-photon microscopy to depths of 1 mm. The resulting two-photon 3D image stack could be analyzed quantitatively to determine the microvascular density as a function of depth. The region examined corresponded to the part of the somatosensory cortex where the forepaw stimulus response was observed in-vivo.

Fig. 4B shows the 2-photon x–z projection of the vasculature in the region indicated in the x–y stack in Fig. 4A. Fig. 4C shows a plot of the capillary density from the vascular cast as a function of depth. The depth profile of the capillary and venous regions identified from their 3D dynamic behavior in-vivo (using LOT) for 2 rats are overlaid. The small surface vein in the vascular cast corresponds to the shallow spike in the black trace in Fig. 4C. The LOT venous traces (blue) represent cross sections through a much larger draining vein, which from the cast images have diameters

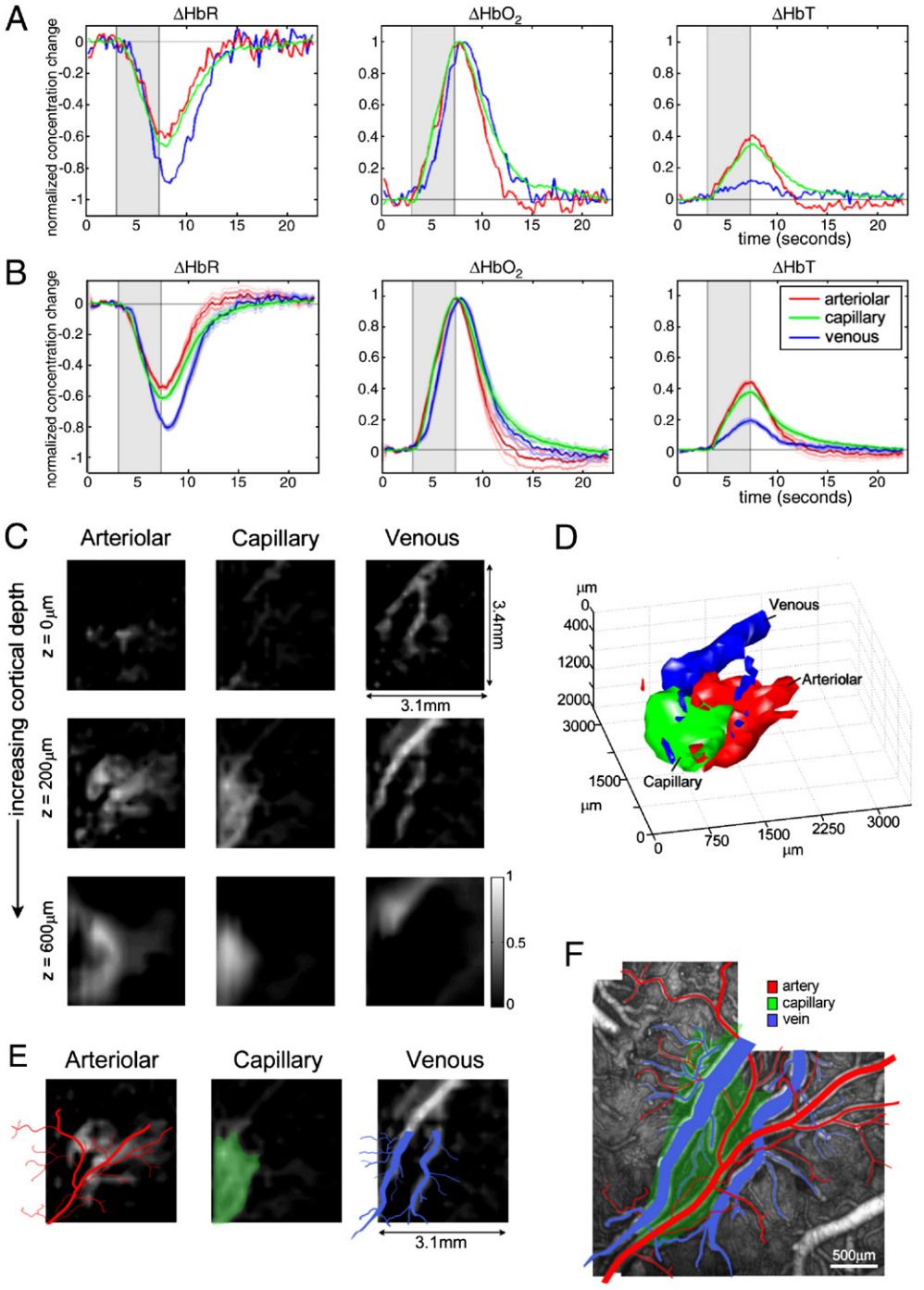

Fig. 3. 3D spatiotemporal separation of vascular compartments. (A) The hemodynamic time-courses from voxels labeled a, v and c in Fig. 2, representing arteriolar, capillary and venous contributions respectively (normalized to the peak HbO_2 value for each compartment). (B) Equivalent time courses, averaged over five rats (standard error on the mean error bounds are shown). (C) Spatiotemporal components extracted from the 3D LOT data shown in Fig. 2B. Gray scale represents the amplitude of the component in each voxel that varies according to the arteriolar, capillary and venous functional time-courses shown in panel A. (D) 3D rendering of LOT vascular compartments (40% isosurface) in panel C. (F) Ex-vivo two-photon image stack of fluorescent vascular cast with veins (blue) and arteries/arterioles (red) identified. (E) 200 μm depth slice from panel C overlaid with the tracing of the arteries (red) and veins (blue) from the vascular cast (after linear rotation and scaling). The capillary response from the LOT results is overlaid onto the vascular cast image to indicate the position of the active underlying capillary bed (green).

approaching 200 μm, suggesting good agreement between the vascular cast and the LOT venous results. In addition, both capillary traces agree well with the vascular density profile, within the limits of the LOT image *z*-resolution. These capillary depth profiles also agree well with published profiles for microvascular density in rat somatosensory cortex (Masamoto et al., 2003).

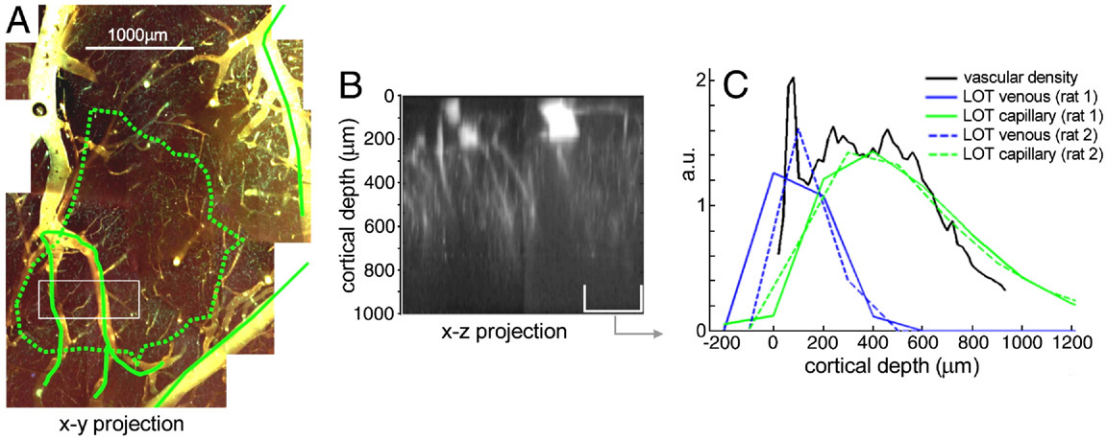

Fig. 4. Depth-resolved validation using in-vitro two-photon microscopy. (A) 2-photon image stack (to depth of 1 mm) of macerated rhodamine-doped vascular cast in the region corresponding to forepaw stimulus response (denoted by green dotted line). (B) *x–z* projection of region indicated in panel A showing superficial vessels, diving venules and arterioles and capillaries. (C) Depth-resolved comparison of LOT venous (blue) and capillary (green) components for two rats with depth-resolved vascular density (black) from *x–z* projection of 2-photon image in the region indicated.

Achieving spatial isolation of the capillary compartment response is strongly motivated by the hypothesis that the location and amplitude of the hemodynamic response in the capillaries will relate more closely to neuronal activation (Malonek and Grinvald, 1996; Woolsey et al., 1996). We have demonstrated good spatial correlation between the 3D structure of the vascular architecture and the LOT-segmented 3D vascular compartments identified *only* from their dynamic behavior. This confirms that spatiotemporal separation is a potentially powerful technique for delineating the hemodynamic response into its vascular compartment distributions. The distinct differences in the venous, capillary and arteriolar responses, even if only HbR changes are considered, suggest that spatiotemporal segmentation of the functional response could provide significant improvements to other functional imaging techniques including 2D optical imaging and fMRI (Berwick et al., 2005; Krings et al., 1999; Yacoub et al., 2006; Zwart et al., 2005).

Summary of the temporal features of the vascular compartments

The robust spatial correspondence between the static vascular architecture and the compartments identified only from their dynaõmic timecourses strongly supports the assertion that the timecourses used for the spatiotemporal separation are indeed representative of the distinct characteristics of the vascular compartments. We can therefore examine both the spatial distributions and the corresponding distinctive timecourses of each vascular compartment to begin to resolve how the hemodynamic response evolves and is controlled.

Fig. 5 illustrates the key features of the average temporal responses of each vascular compartment (over 5 rats). This data is shown in closer detail and with error bounds in the supplementary data (Figs. S5 and S6). Each plot compares timecourses normalized to their peak, to accentuate the differences in the timing of the onsets and decays of the responses. The bar graphs provide summaries of the relative onset times, amplitudes and the fractional contribution of each compartment to the overall hemodynamic response. Details on the methods used for parameter extraction are provided in the supplementary data.

The arteriolar response exhibits prompt onset and prompt post-stimulus decay, with a small undershoot (labeled (i) in Fig. 5D). This temporal pattern is seen for all hemoglobin types and closely resembles previously reported *blood flow* timecourses in rat during somatosensory stimulus (Jones et al., 2001). This relation is investigated further below. We also note that a measurable change in HbR is seen in the arteriolar compartment (53±4% of arteriolar HbO_2 change, $p=0.01$, paired *t*-test, $n=5$), suggesting that initial hemoglobin oxygen saturation in branching arterioles is less than 98%. This is in agreement with PO_2 measurements of branching arterioles in rat cortex (Vovenko, 1999), and in hamster cheek pouch (Duling and Berne, 1970a), and the findings of (Berwick et al., 2005; Zheng et al., 2005), although it is contrary to the assumption that arterioles do not contribute to the BOLD signal in fMRI (see also Fig. 5I).

The delayed onset of HbR and HbO_2 in the veins relative to the arterioles and capillaries is an obvious feature ($\Delta t_{30\%}=0.57\pm0.22$ s, $p<0.01$, labeled (ii) in Fig. 5B). This is a well documented phenomenon caused by the time taken for changes in arterial flow to affect the oxygenation state of the venous out-flow, and is related to the capillary transit time and changes in oxygen extraction fraction. However, the HbT change in the veins (which is small: 10±3% of the total HbT change, $p<0.016$, in agreement with (Berwick et al., 2005) and (Vanzetta et al., 2005)), does not exhibit a significant *delay* relative to HbT changes in the arteriolar and capillary compartments ($p>0.5$ at 30% max, labeled (iii) in Fig. 5C). The small amplitude and prompt onset of HbT changes in the venous compartment are contradictory to standing basic assumptions applied to fMRI interpretation which assume that the majority of HbT and HbR changes occur in the veins and are uniformly delayed (Marota et al., 1999). This is investigated further below.

Another notable feature is the latency of the capillary bed post-stimulus decay (labeled iv in Fig. 5C and v in Fig. 5F). At 50% max post-stimulus, $t_{cap}-t_{vein}=0.61\pm0.54$ s, $p=0.03$. The capillary compartment (given by the voxels responding with capillary-like dynamics) also composes the largest fraction of the overall hemodynamic signal for all hemoglobin types, as shown in Fig. 5I.

Temporal validation: in-vivo two-photon microscopy of vascular dynamics

In order to validate our interpretation of the dynamic timecourses from LOT, we used in-vivo two-photon microscopy

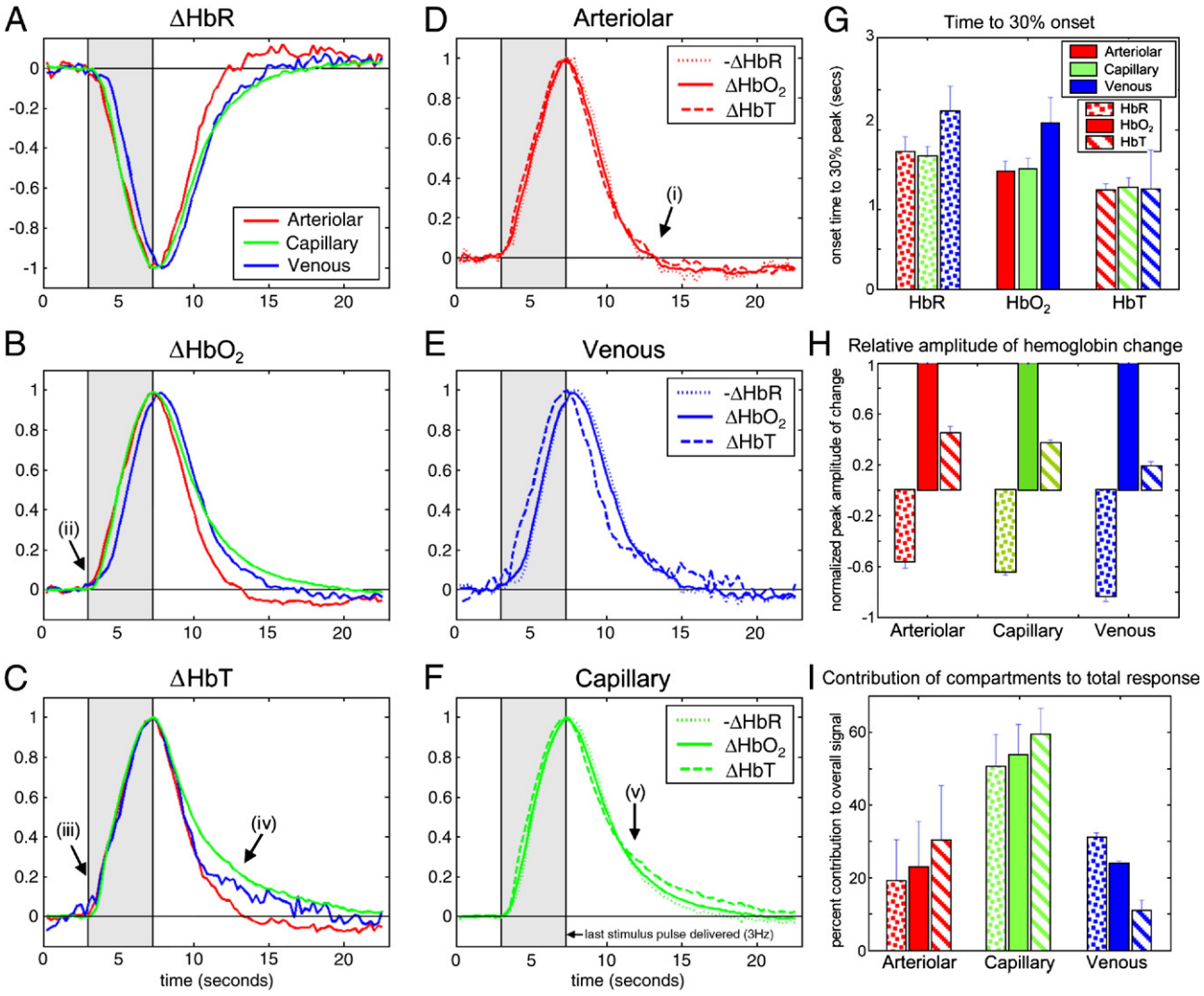

Fig. 5. Analysis of vascular compartment time-course dynamics. The timecourses extracted from LOT data for each hemoglobin type (A–C) and vascular compartment (D–F) and are shown normalized to their peak to accentuate onset and decay timing trends. (G) Shows time to 30% onset for each hemoglobin type within each compartment. In all cases HbT changes first, followed by HbO_2 and then HbR ($p<0.03$ for all compartments). Note that the same trend is seen in the post-stimulus decay to 70% of the peak ($p<0.013$). Venous onset is after both arteriolar and capillary for HbO_2 and HbR ($p<0.02$). (H) Shows trends in the relative amplitudes of the responses (normalized to the HbO_2 response of each compartment). All differences are significant with $p<0.016$. (I) Shows the relative percentage contribution of each vascular compartment to the overall hemodynamic response. This data was calculated with data from 3 rats whose cranial windows were large enough to visualize all major feeding and draining vessels. Note the large overall capillary contribution, the small venous HbT contribution and the large arteriole HbR contribution. Features labeled i–v are described in the text. Error bars on panels G, H and I show standard deviation. Methods used for parameter extraction are described in the supplemental data.

to investigate the following two aspects of the hemodynamic response: 1) The possible direct correspondence between arteriolar HbT and blood flow changes, offering insights into the control mechanisms of the hemodynamic response, and as a potentially new way to infer blood flow, and 2) the mechanism of the small change in venous HbT for short (4 s) stimuli, since the general assumptions in fMRI analysis (where longer stimuli are usually considered) is that the majority of the BOLD and cerebral blood volume (CBV) changes are due to a significant dilation/ballooning of the veins (Buxton et al., 1998; Hoge et al., 1999; Kong et al., 2004; Mandeville et al., 1999; Zheng et al., 2005).

For each rat, we focused our in-vivo two-photon measurements on the area responding to a 4 s forepaw stimulus (defined by CCD-based HbT imaging prior to microscopy, as illustrated in Fig. 6A). 180×180 μm images were acquired at 14 frames per second during stimulation to simultaneously capture movies of the dynamics of both the arterioles and veins within the responding area. Each stimulus block was repeated 3 to 5 times, and up to 15 different fields of view were studied to cover the active area. Consistent results were seen in all rats studied. We present data from the animal for which the most sites within the active area were reliably and repeatedly measured. The image series were processed as described in supplementary data Fig. S7.

Our results confirm that for a 4 s forepaw stimulus: 1) The arterioles dilate significantly in response to stimulus (Figs. 6C and D), and constrict with a small undershoot following stimulus cessation: a timecourse consistent with our previous LOT

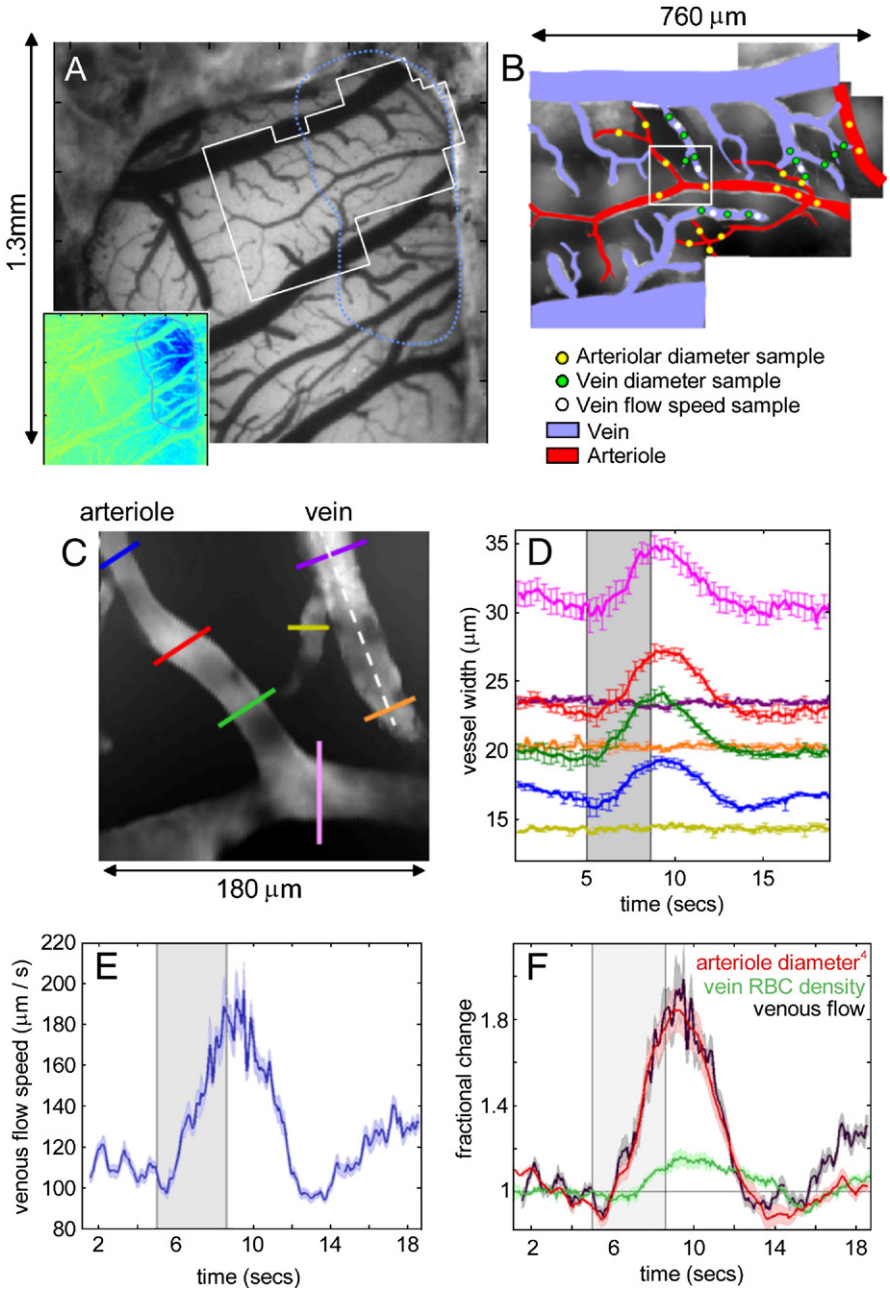

Fig. 6. In-vivo two photon microscopy of vascular compartments. (A) The exposed cortex imaged using a CCD camera at 570 nm. Inset shows the region responding to 4 s forepaw stimulation. White outline illustrates region examined using in-vivo two-photon microscopy as shown in the montage B. Arterioles and veins are color coded red and blue. Dots illustrate the locations of the quantitative measures given in Table 1. (C) Shows a representative single field of view from panel A (180 × 180 μm) containing both an arteriole and a venule. The area was imaged at 14 frames per second for 20 s while a 4 s forepaw stimulus was delivered. The vessel diameters at the points indicated by the colored lines on panel C are shown in panel D as a function of time (average of 4 stimulus repetitions, error bars show standard error). Note that no significant change in the diameter of the venule is seen. (E) Shows the speed of red blood cells in the venule along the white dotted line in panel C for the *same* 4 stimulus repetitions (error bounds show the standard error on the mean). (F) (red) Shows the fractional change in the 4th power of the mean arteriolar dilation in panel C (proportional to flow by Poiseuille's law) (green) the fractional change in the red blood cell density in the venule in panel C, and the fractional change in venous flow (black), given by the speed change (from E) multiplied by the RBC density change. Error bounds show the standard error on the mean. Note that all parameters (venous flow, speed, arteriolar dilation and RBC density) were evaluated simultaneously over the same 4 stimulus repetitions.

arteriolar HbT changes (Fig. 5D). 2) A measurable diameter increase was not observed in the veins in response to a short 4 s forepaw stimulus (Fig. 6D). In addition, we were able to observe an increase in the *speed* of the flow in the veins (Fig. 6E). In 40% of the veins examined, a slightly delayed increase in red blood cell (RBC) density was also noted (17 ± 6% where seen and 6.4 ± 8.6% overall change, at cessation of stimulus) as shown in Fig. 6F. These trends were consistent across all rats. Table 1 summarizes the mean changes over the whole active region illustrated in Fig. 6B.

Table 1
Parameters of vascular dynamics across the active region shown in Fig. 6B during 4 s forepaw stimulus

	Arterioles	Venules
Diameter change (%)	16.8±5.5% (n=109)	−0.15±0.72% (n=28)
Resting diameter	19±8 μm (6.5 to 39 μm)	31±10 μm (20 to 61 μm)
RBC density change (%)	[a]	6.4±8.6% (n=5)
Resting RBC density	55±4% (n=5)	46±4% (n=5)
Speed change (%)	[b]	34.0±13.5% (n=5)
Resting speed	[b]	105±36 μm s^{-1} (57–152 μm s^{-1})
Flow change (%)	[b]	53±17% (n=5)

Data were acquired using rapid full-field two-photon microscopy (data processing methods are described in Supplementary data Fig. S7). (n) describes the number of sites examined, with 4 stimulus repetitions at each site.

[a] RBC density changes not measurable in dilating arterioles due to depth-of-field effects.

[b] Arteriolar speed is too fast to measure with our current acquisition rate.

For our paradigm therefore, the arterioles dilate and a concomitant increase in blood flow is seen in the veins. This increase in flow manifests primarily as a change in the *speed* of the blood flow in the veins, sometimes accompanied by a small delayed increase in the venous RBC density, and not as a significant venous dilation or stretching. This red blood cell density change may account for the small HbT change that we observed in the veins in our LOT results, particularly the latent tail of the venous HbT increase. It is possible that the early changes in the LOT venous HbT *are* the result of a very small venous diameter increase, below our measurement threshold. This slight % change might correspond to the increased inflow pressure, and would be expected to vary with the arteriolar dilation. Note that further studies are required to determine whether venous dilation becomes a more significant phenomenon for longer or stronger stimuli, for significantly larger veins, or for different species.

As shown in Fig 6F, we find very close correlation (ρ=0.985, y=1.00x+0.03, R^2=0.97) between the percentage changes in the venous flow (RBC density × speed) and the percentage change in diameter^4 of the arteriole (as given by Poiseuille's law). This finding strongly supports the notion that blood flow dynamics may indeed be calculable from measurements of arteriolar HbT.

Discussion

There is widespread disagreement in the literature regarding the physical properties and behavior of the vascular compartments during functional stimulation. Partly, this has arisen from a reliance on historical ex-vivo and in-vitro data, and the combination of conclusions drawn from very different experiments, using different measurement modalities (fMRI, optical, laser Doppler) and stimuli of different types, strengths and durations. Our extraction of the individual timecourses of HbR, HbO_2 and HbT in the different vascular compartments in rat somatosensory cortex during a 4 s forepaw stimulus provides the first delineated observations of the whole timecourse and the whole 3D active field measured simultaneously in-vivo. Our results agree with almost all *observations* of the composite dynamic characteristics of the hemodynamic response. However, our compartment-resolved findings prompt reinvestigation of some of the mechanisms underlying the dynamic features of the functional response:

Vascular compliance and capillary hyperemia

Our results suggest that a 4 s forepaw stimulus causes a gradual and near simultaneous increase in HbT throughout the vascular compartments (with a small change in the veins and a large change in the capillary bed). Following stimulus cessation, the HbT in the arterioles drops rapidly, the capillary HbT decays slowly, and the venous HbT exhibits a biphasic decay; initially similar to the arteriolar decay and then to the capillary decay. These observations imply that there is significant hyperemia in the capillary bed.

Hyperemia in the capillary bed has been observed by others including (Schulte et al., 2003) and (Villringer et al., 1994), and an HbT change in the parenchyma is routinely seen in optical imaging studies (Culver et al., 2005; Devor et al., 2003; Jones et al., 2001; Nemoto et al., 2004; Sheth et al., 2004; Vanzetta et al., 2005). Nevertheless, the mechanism by which the capillary bed can increase its net hemoglobin concentration remains controversial, and so most mathematical models of cortical hemodynamics continue to assume that CBV and HbT in the capillary bed cannot change (Buxton et al., 1998; Hoge et al., 1999; Kong et al., 2004; Mandeville et al., 1999; Zheng et al., 2005).

Our findings agree well with the observations of (Villringer et al., 1994), who used in-vivo confocal microscopy of fluorescein-perfused cortical capillaries to study 'capillary recruitment' versus 'capillary population changes' (or *functional* recruitment). Consistent with the latter, they found that in a resting state, some capillaries exhibited low or no RBC flow, and some (while having plasma flow) did not contain RBCs. During hypercapnia RBC speed and flux increased, along with an increase in homogeneity of flow and a reduction in the number of poorly perfused capillaries. An increase in capillary diameter from 5.33±0.25 to 5.66±0.29 μm was also observed. Similar capillary dilations in response to hypercapnia were recently observed using two-photon microscopy by Hutchinson et al. (2006).

Capillary dynamics during somatosensory stimulus in-vivo have not yet been fully explored in detail. Based on our observations, we hypothesize that the mechanism for the capillary bed hyperemia that we observe is a net increase in the number of red blood cells per capillary (the RBC linear density). While increases in capillary diameter are thought to occur during stimulus response (either passively or actively (Harrison et al., 2002; Peppiatt et al., 2005)), in such conditions the capillaries are highly unlikely to dilate/expand sufficiently to allow more than one RBC to pass at the same time. Diameter increases may therefore serve to allow a higher volume of plasma flow around the RBCs, which could result in an increase in RBC stacking linear density.

Positive correlation between capillary flow and linear density was seen at rest in olfactory glomeruli by Chaigneau et al., and increases in flow, speed and linear density were observed in a subset of capillaries during stimulus response (Chaigneau et al., 2003). Kleinfeld et al. studied a single capillary during somatosensory hindpaw stimulus, observing a speed increase and a very slight *decrease* in the linear density of the RBCs (Kleinfeld et al., 1998). However, Villringer et al. and Chaigneau et al.'s results demonstrate that it is very difficult to infer the ensemble response from the behavior of a single capillary. Barfod et al. (1997) used laser Doppler to independently measure the 'concentration' and 'velocity' of moving blood cells in the cerebellum

during hypercapnia and electrical cortical stimulus. They found trends similar to our venous RBC density and venous flow changes, concluding that they were observing 'functional recruitment' in the capillary bed. Based on our data and the strong evidence from optical imaging that capillary hyperemia does occur, we suggest that a net increase in the linear density of RBCs in the capillaries accompanies the flow response to functional stimulus.

Our results also suggest that any vascular network resistance changes are time-varying on a relatively slow timescale. Our observation that venous HbT increases almost simultaneously with the capillary and arteriolar HbT suggests that a 'pressure wave' caused by the flow increase propagates through the system rapidly. Therefore, we expect that the build up of RBCs in the capillary bed occurs gradually alongside arteriolar dilation and blood flow increases.

This hyperemia mechanism is also supported by the decay dynamics of the HbT response in the compartments. As shown in both our LOT and two-photon results, the arteriolar response rapidly returns to baseline after cessation of the stimulus, thereby reducing overall flow (consistent with the observations of (Jones et al., 2001)). However, the capillary HbT decay is much slower. We hypothesize that the RBCs that have built up throughout the capillary bed, with high plasma flow, begin to experience a reduction in flow and pressure and a consequent decrease in capillary diameter. Removal of these extra RBCs is then likely to take longer in low flow conditions since resistance has increased. The latent increase in venous RBC density in our two-photon results (Fig. 6F) may be illustrating this delayed wash-out of extra RBCs from the capillary bed. This mechanism is also supported by the biphasic HbT decay of the venous compartment in our LOT results, which we believe initially reflects the reduction in arteriolar diameter and therefore flow or pressure, and then matches the rate of outflow of the extra RBCs from the capillaries (labeled (iv) in Fig. 5C).

This biphasic pattern has also been observed in optical and fMRI data of CBV relative to Laser Doppler measurements of cerebral blood flow in rats (for 2 (slight effect) and 20 s whisker pad stimulus (Kong et al., 2004), and 6 and 30 s hindpaw stimulus (Mandeville et al., 1999)). The explanation suggested for the origin of the biphasic pattern was a non-linear expansion in the venous compartment as described in the windkessel modification (Mandeville et al., 1999) to the balloon model (Buxton et al., 1998). In (Kong et al., 2004)'s 'Modified windkessel Model with Compliance', better correspondence with measured data was found when the compliance was allowed to be delayed and time-varying. Without a satisfactory mechanism for capillary hyperemia, fMRI literature has been conflicted on the presence of a significant CBV change in the capillary bed. We suggest that in fact this extra compliance factor *is* a feature of the capillary bed and not the veins, and that a significant fraction of the CBV change occurs in the capillary compartment. Interestingly, many fMRI results support localization of CBV changes to the deeper capillary bed layers of the cortex (Goense and Logothetis, 2006; Harel et al., 2006; Lu et al., 2004; Mandeville et al., 1998; Marota et al., 1999; Zhao et al., 2006). The BOLD post-stimulus undershoot (Mandeville et al., 1999) would also be better explained by an increase in oxygen extraction fraction within the capillary bed, where oxygen perfusion is optimized, rather than in the venous compartment. Further investigation is required to determine whether venous expansion becomes a significant effect for longer stimuli. However, this interpretation of our results is strongly supported by the findings and analysis presented by (Yacoub et al., 2006), who observe similar trends including decay latency between capillary bed BOLD and CBV response using high-resolution depth-resolved fMRI in cats.

Active or passive vascular mechanisms?

A related question regarding the mechanisms of the hemodynamic response concerns which parts of the vascular dynamics are active or passive. It is not yet understood how certain arterioles and capillaries 'know' that they must form part of a route for increasing blood flow to only a localized neuronally active area.

Roy and Sherrington (1890) originally suggested that diffusion of the by-products of metabolism caused retrograde vasodilatation of feeding vessels. However, it is now generally accepted that diffusion is too slow over such distances (>1 mm), and circulating fresh CSF over pial arterioles does not prevent them from responding to somatosensory stimulus (Ngai and Winn, 2002). An increase in intraluminal arteriolar flow caused by an active reduction in capillary resistance was also suggested as a mechanism that could trigger a passive arteriolar dilation via sheer-stress changes (Ngai and Winn, 1995). However, this mechanism would result in distinctive speed of flow changes, and veins would have a delayed speed and HbT increase (features that we do not observe in our data).

Remaining theories assume either that: a signal is somehow propagated retrograde from the capillary bed via the vasculature itself, or that a signal is directly communicated to the pial arterioles via a neuronal or glial network. As evidence for each, attention has focused on trying to measure the *direction* of the propagation of vasodilation (Iadecola et al., 1997; Sheth et al., 2005; Vanzetta et al., 2005).

To date, retrograde propagation of arteriolar dilation has not been directly observed in the cortex in response somatosensory stimulus. However, supporting observations include retrograde vasodilation in rat cerebellum arterioles following direct electrical stimulus of the parallel fibers (Iadecola et al., 1997) and the dilation and constriction of isolated rat cerebral penetrating arterioles in response to ATP (Dietrich et al., 1996). Other evidence includes; dilation of upstream arterioles in striated muscle in response to local stimulation (Berg et al., 1997), and bidirectional propagation of dilation at 200 μm/s in hamster cheek pouch arterioles in response to local acetylcholine (Duling and Berne, 1970b). At 200 um/s, we would expect to be able to see propagation of vasodilation in the arterioles in our two-photon results. Also, if retrograde dilation is so slow, we might also expect capillary HbT or flow changes to significantly precede changes in more distant arterioles.

However, the mechanisms controlling propagation of vasodilation in cerebral vessels have yet to be determined, and may involve the vascular endothelium, smooth muscle cells, or perivascular nerves (Andresen et al., 2006; Fahrenkrug et al., 2000; Girouard and Iadecola, 2006; Iadecola, 1993; Lou et al., 1987; Welsh and Segal, 1998). The mechanisms contributing to previously observed propagations may not be the same in each case.

A possible faster mechanism might involve hyperpolarization of the vascular membranes local to the neuronal activity resulting in vasodilatory signals being propagated through the vasculature via the cellular path of least resistance to upstream feeding vessels. If a rapid electrical signaling pathway exists, it is possible that a source-sink model could trace its path before any vascular motion occurred. In this case, the gradual movement of the dilation site along the vessel (as in hamster cheek pouch) is not likely to be observable, and dilation would instead appear to begin

instantaneously along the entire path. This model is well supported by the multiple-whisker stimulation data in Erinjeri and Woolsey (2002), and would also provide an elegant mechanism for identifying and modulating only those vessels composing the most direct route to a supplying large vessel.

The seemingly opposing view to retrograde vasodilation is that arteriolar dilation might be triggered by a neuronal or glial network reaching to specific distant parts of the vascular tree feeding the neuronally active area (Staiger et al., 1996; Vanzetta et al., 2005). In this case, initiation of the dilation would not be limited by the possibly slow propagation speeds of retrograde vasodilation, and could even receive direct contributions from other areas such as the thalamus (Iadecola, 1993; Staiger et al., 1996). It is likely that some local propagation of dilation would still be required, since neuronal or glial connections and smooth muscle or pericyte locations are likely to be discrete. While evidence is mounting that interneurons and glia can actively cause both vasodilation and vasoconstriction (Cauli et al., 2004; Girouard and Iadecola, 2006; Hamel, 2006; Takano et al., 2006; Wang et al., 2006; Zonta et al., 2003), this mechanism would require some predetermined network of vascular connections that can synchronize a specific blood flow response in contrast to the more causal response that retrograde propagation might provide. However, such 'anticipatory' flow control mechanisms have been hypothesized as a cause of the apparent over-supply of oxygen to active areas (Iadecola, 2002).

While at the limits of our current signal to noise, our average HbT traces, in agreement with (Vanzetta et al., 2005), do suggest that arterioles begin changing their HbT slightly before the capillaries (Fig. S5F). Vanzetta et al. cite their findings as evidence for anteriograde propagation of vasodilation, although they also observe that larger arteries respond later than arterioles. Interestingly, our data is also consistent with Sheth et al. (2005)'s observations that the arteriolar response *peaks* after the capillary response, since our HbT times to 30% and 70% (Fig. S5) suggest that the *rate* of arteriolar HbT increase is slower than that of the capillary bed response. Correspondingly, we do not agree with Sheth et al.'s interpretation that this time-to-peak difference is evidence for retrograde propagation of vasodilation.

The rapid propagation of the HbT response (representing a pressure wave) through all compartments also suggests that on measurable timescales, a rapid capillary resistance reduction does not occur substantially before the arteriolar dilation. Note however, that a measurable HbT change in the capillaries would not necessarily develop instantaneously, whether a signal originated there, or if a local active resistance reduction occurred. Therefore, our findings are consistent with either a very rapid retrograde transduction of a vasodilatory signal via the vessels themselves, or rapid triggering of vasodilation and constriction via a neuronal and/or glial network. We do not see evidence supporting a slow retrograde propagation of vasodilation.

In our two-photon microscopy results, we also find that the timing of onset of vasodilation and constriction (while variable) is distributed fairly uniformly over the length of all of the arterioles (Fig. 6D), and does not appear to exhibit a measurable unidirectional propagation of dilation onset (sampling a 180×180 μm area at 14 frames per second). Also, unlike the cortical stimulus results of (Iadecola et al., 1997) in the cerebellum, we also did not observe any correlation with initial arteriolar size, and the percentage diameter increase ($R^2 = 0.07$, for 109 arteriole locations between 6.5. and 36 μm diameter). Note that further investigation is required to independently examine the relation between onset and decay both with vessel diameter *and* with distance from the focus of the active region.

Further insight into the vasodilation propagation mechanism is found in our observed decay dynamics. Upon cessation of stimulus, the arterioles rapidly reduce their diameters, whereas the capillaries retain their higher HbT for an extended period. The capillaries therefore are unlikely to be causing an active flow decrease that can send a signal to trigger arteriolar constriction as suggested by Ngai and Winn (1995) and Duling and Berne (1970a). Instead, these results suggest the presence of an established communication network (be it neuronal, glial or within the vasculature) that allows the responding neurons to rapidly relay back to the dilated arterioles that increased flow is no longer required, without causing measurable changes in the capillary bed first. While it is possible that different mechanisms control onset and decay, if a network is in place for initiating the decay of the hemodynamic response, then it is possible that it is utilized during the onset.

The presence of controlling structures on both capillaries and arterioles and has been noted in several vascular cast studies (Harrison et al., 2002; Rodriguez-Baeza et al., 1998; Toribatakea et al., 1997). Active responses to vasoconstrictors and vasodilators have been observed in microvasculature in cortical brain slices (Cauli et al., 2004) and in capillaries in the cerebellum and retina (Peppiatt et al., 2006). We expect that controlled changes in pre-capillary arterioles and perhaps capillary diameters indeed play an important role in increasing RBC flow to the neuronally active area. However, we propose that rather than controlling and triggering overall flow responses, that observed sphincters and pericytes fine-tune and optimize the capillary bed flow, either via local vasoactive mediators *or* neuro/glial networks. It is also likely that some structures are present to report intraluminal pressure/vessel diameter as a feedback mechanism.

Our data therefore suggests that capillary hyperemia contributes significantly to measured HbT and CBV changes, and is consistent with a mechanism whereby RBCs increase their linear densities at higher flow rates. We do not find evidence for slow retrograde *or* anteriograde vasodilation in pial arterioles. Instead, the onset of vasodilation seems to occur via rapid transduction of a signal from the active area, either via fast transmission along the vascular tree or via a neuron/glial network.

Methodological conclusions: spatiotemporal fitting and 3D imaging

We have demonstrated that it is possible to delineate the vascular compartments within the hemodynamic response based only on their differing hemodynamic timecourses. These time-courses were further shown to be robust signatures with physiologically relevant and significant features. We assert that this approach is a potentially useful tool for enhancement of resolution of functional imaging modalities that generally consider the entire hemodynamic response as a single, average localized hemodynamic change.

Since neuronal activity is widely assumed to spatially correlate most closely to the capillary bed response, improving localization of signals to the capillary bed could overcome the problems of distortion caused by HbR changes in distant draining veins in fMRI (Turner, 2002). Automated algorithms to enhance localization in 2D optical imaging have previously been proposed

(Mayhew et al., 1998; Zheng et al., 2001). However, by basing our algorithm solely on the differing physical characteristics of the vascular compartments, we constrain our separation in a physiologically meaningful way. A significant benefit is that, while isolating the capillary response, we also identify the potentially very useful arteriolar and venous spatial extents and timecourses. While our analysis utilized HbO_2, HbR and HbT timecourses together to distinguish between the 3 major vascular compartments, we expect that with sufficient temporal resolution and signal to noise that similar separation could be achieved using only the BOLD signal in fMRI (Krings et al., 1999; Zwart et al., 2005). Temporal characteristics of both the onset and decay dynamics are sufficiently distinctive that basis timecourses could be derived from the data itself, in a similar way to our 'subjective masking' (see supplemental data figure S3 and Zwart et al., 2005).

Our finding that arteriolar dilation measurements provide strong correlations with venous flow changes also suggests that isolation of the arteriolar hemodynamics from CBV, optical imaging or even BOLD (since we see HbR changes in the arterioles), could provide a simultaneous measure of blood flow. In some cases, this approach may provide an alternative to using a second modality (such as laser Doppler, arterial spin labeling MRI or laser speckle imaging) for derivation of parameters such as the Cerebral Metabolic Rate of Oxygen Consumption (Dunn et al., 2003; Hoge et al., 1999; Jones et al., 2001).

3D LOT imaging of the hemodynamic response greatly aided in isolation of the compartment-specific responses. Visualization of compartmentalized data in 3D helped to validate that the temporal dynamics indeed localized to vasculature in anatomically consistent locations. Our 3D imaging results also suggest that superficially weighted 2D optical imaging underestimates the amplitude of the capillary response in relation to the superficial arteriolar and venous signals (Berwick et al., 2005; Vanzetta et al., 2005). We plan to utilize LOT to further explore the 3D hemodynamics of the capillary beds alongside investigation of the 3D neuronal response to stimulus using calcium and voltage sensitive dyes.

To date, there has been a reliance on parametric comparisons of neuronal and hemodynamic responses to stimulus to formulate models of the neurovascular response. We have used modern imaging tools to investigate the hemodynamic response in closer detail. Determining the neuronal and vascular mechanisms that underlie the observed ensemble hemodynamic response is an essential step towards the development of more reliable and versatile tools for interpretation of the hemodynamic measures such as fMRI.

Acknowledgments

This work was funded by R21NS053684, R01EB000790, K25NS41291, R01EB000768, R01NS05118 and The Whitaker Foundation and the Wallace H Coulter Foundation. The authors wish to thank Svetlana Ruvinskaya, Alan Koretsky, Alfonso Silva, Britton Chance, Edith Hamel, Bruno Cauli, Noam Harel, Joseph Mandeville, Jens Steinbrink, David Attwell, Nozomi Nishimura and David Kleinfeld for useful advice and discussions.

Appendix A. Supplementary data

Supplementary data associated with this article can be found, in the online version, at doi:10.1016/j.neuroimage.2006.11.032.

References

Andresen, J., Shafi, N.I., Bryan Jr., R.M., 2006. Endothelial influences on cerebrovascular tone. J. Appl. Physiol. 100 (1), 318–327.

Arridge, S.R., 1999. Optical tomography in medical imaging. Inverse Probl. 15, 41–93.

Arthurs, O.J., Boniface, S., 2002. How well do we understand the neural origins of the fMRI BOLD signal? Trends Neurosci. 25 (1), 27–31.

Attwell, D., Iadecola, C., 2002. The neural basis of functional brain imaging signals. Trends Neurosci. 25 (12), 621–625.

Barfod, C., Akgoren, N., Fabricius, M., Dirnagl, U., Lauritzen, M., 1997. Laser–Doppler measurements of concentration and velocity of moving blood cells in rat cerebral circulation. Acta Physiol. Scand. 160 (2), 123–132.

Belliveau, J.W., Kennedy, D.N., McKinstry, R.C., Buchbinder, B.R., Weisskoff, R.M., Cohen, M.S., Vevea, J.M., Brady, T.J., Rosen, B.R., 1991. Functional mapping of the human visual cortex by magnetic resonance imaging. Science 254 (5032), 716–719.

Berg, B.R., Cohen, K.D., Sarelius, I.H., 1997. Direct coupling between blood flow and metabolism at the capillary level in striated muscle. Am. J. Physiol.: Heart Circ. Physiol. 272 (6), H2693–H2700.

Berwick, J., Johnston, D., Jones, M., Martindale, J., Redgrave, P., McLoughlin, N., Schiessl, I., Mayhew, J.E.W., 2005. Neurovascular coupling investigated with two-dimensional optical imaging spectroscopy in rat whisker barrel cortex. Eur. J. Neurosci. 22 (7), 1655–1666.

Bouchard, M., Ruvinskya, L., Boas, D.A., Hillman, E.M.C., 2006. Video-rate two-photon microscopy of cortical hemodynamics in-vivo. BIOMED Proceedings, OSA Technical Digest.

Brecht, M., Roth, A., Sakmann, B., 2003. Dynamic receptive fields of reconstructed pyramidal cells in layers 3 and 2 of rat somatosensory barrel cortex. J. Physiol. 553 (Pt. 1), 243–265.

Buxton, R.B., Wong, E.C., Frank, L.R., 1998. Dynamics of blood flow and oxygenation changes during brain activation: the balloon model. Magn. Reson. Med. 39, 855–864.

Cauli, B., Tong, X.-K., Rancillac, A., Serluca, N., Lambolez, B., Rossier, J., Hamel, E., 2004. Cortical GABA interneurons in neurovascular coupling: relays for subcortical vasoactive pathways. J. Neurosci. 24 (41), 8940–8949.

Chaigneau, E., Oheim, M., Audinat, E., Charpak, S., 2003. Two-photon imaging of capillary blood flow in olfactory bulb glomeruli. Proc. Natl. Acad. Sci. 100 (22), 13081–13086.

Culver, J.P., Siegel, A.M., Franceschini, M.A., Mandeville, J.B., Boas, D.A., 2005. Evidence that cerebral blood volume can provide brain activation maps with better spatial resolution than deoxyhemoglobin. NeuroImage 27, 947–959.

Devor, A., Dunn, A.K., Andermann, M.L., Ulbert, I., Boas, D.A., Dale, A.M., 2003. Coupling of total hemoglobin concentration, oxygenation, and neural activity in rat somatosensory cortex. Neuron 39 (2), 353–359.

Dietrich, H.H., Kajita, Y., Dacey Jr., R.G., 1996. Local and conducted vasomotor responses in isolated rat cerebral arterioles. Am. J. Physiol.: Heart Circ. Physiol. 271 (3), H1109–H1116.

Duling, B.R., Berne, R.M., 1970a. Longitudinal gradients in periarteriolar oxygen tension: a possible mechanism for the participation of oxygen in local regulation of blood flow. Circ. Res. 27, 669–678.

Duling, B.R., Berne, R.M., 1970b. Propagated vasodilation in the microcirculation of the hamster cheek pouch. Circ. Res. 26 (2), 163–170.

Dunn, A.K., Boas, D.A., 2000. Transport-based image reconstruction in turbid media with small source–detector separations. Opt. Lett. 25 (24), 1777–1779.

Dunn, A., Devor, A., Andermann, M., Bolay, H., Moskowitz, M., Dale, A., Boas, D., 2003. Simultaneous imaging of total cerebral hemoglobin concentration, oxygenation and blood flow during functional activation. Opt. Lett. 28pp, 28–30.

Erinjeri, J.P., Woolsey, T.A., 2002. Spatial integration of vascular changes with neural activity in mouse cortex. J. Cereb. Blood Flow Metab. 22 (3), 353–360.

Fahrenkrug, J., Hannibal, J., Tams, J., Georg, B., 2000. Immunohistochemical localization of the VIP1 receptor (VPAC1R) in rat cerebral blood vessels: relation to PACAP and VIP containing nerves. J. Cereb. Blood Flow Metab. 20, 1205–1214.

Fox, P.T., Raichle, M.E., 1986. Focal physiological uncoupling of cerebral blood flow and oxidative metabolism during somatosensory stimulation in human subjects. Proc. Natl. Acad. Sci. 83, 1140–1144.

Girouard, H., Iadecola, C., 2006. Neurovascular coupling in the normal brain and in hypertension, stroke, and Alzheimer disease. J. Appl. Physiol. 100 (1), 328–335.

Goense, J.B., Logothetis, N.K., 2006. Laminar specificity in monkey V1 using high-resolution SE-fMRI. Magn. Reson. Imaging 24 (4), 381–392.

Hamel, E., 2006. Perivascular nerves and the regulation of cerebrovascular tone. J. Appl. Physiol. 100 (3), 1059–1064.

Harel, N., Lin, J., Moeller, S., Ugurbil, K., Yacoub, E., 2006. Combined imaging–histological study of cortical laminar specificity of fMRI signals. NeuroImage 29 (3), 879–887.

Harrison, R.V., Harel, N., Panesar, J., Mount, R.J., 2002. Blood capillary distribution correlates with hemodynamic based functional imaging in cerebral cortex. Cereb. Cortex 12, 225–233.

Hewson-Stoate, N., Jones, M., Martindale, J., Berwick, J., Mayhew, J., 2005. Further nonlinearities in neurovascular coupling in rodent barrel cortex. NeuroImage 24, 565–574.

Hillman, E.M.C., 2002. Experimental and theoretical investigations of near infrared tomographic imaging methods and clinical applications (PhD thesis), in Department of Medical Physics and Bioengineering, University College. University of London: London.

Hillman, E.M.C., Boas, D.A., Dale, A.M., Dunn, A.K., 2004. Laminar optical tomography: demonstration of millimeter-scale depth-resolved imaging in turbid media. Opt. Lett. 29 (14), 1650–1652.

Hoge, R.D., Atkinson, J., Gill, B., Crelier, G.R., Marrett, S., Pike, G.B., 1999. Investigation of BOLD signal dependence on cerebral blood flow and oxygen consumption: the deoxyhemoglobin dilution model. Magn. Reson. Med. 42, 849–863.

Hutchinson, E.B., Stefanovic, B., Koretsky, A.P., Silva, A.C., 2006. Spatial flow-volume dissociation of the cerebral microcirculatory response to mild hypercapnia. NeuroImage 32 (2), 520–530.

Iadecola, C., 1993. Regulation of the cerebral microcirculation during neural activity: is nitric oxide the missing link? Trends Neurosci. 16 (6), 206–214.

Iadecola, C., 2002. CC commentary: intrinsic signals and functional brain mapping: caution, blood vessels at work. Cereb. Cortex x12 (3), 223–224.

Iadecola, C., 2004. Neurovascular regulation in the normal brain and in Alzheimer's disease. Nat. Rev. 5, 347–360.

Iadecola, C., Yang, G., Ebner, T.J., Chen, G., 1997. Local and propagated vascular responses evoked by focal synaptic activity in cerebellar cortex. J. Neurophysiol. 78 (2), 651–659.

Jones, M., Berwick, J., Johnston, D., Mayhew, J., 2001. Concurrent optical imaging spectroscopy and laser–Doppler flowmetry: the relationship between blood flow, oxygenation, and volume in rodent barrel cortex. NeuroImage 13, 1002–1015.

Kleinfeld, D., Delaney, K.R., 1996. Distributed representation of vibrissa movement in the upper layers of somatosensory cortex revealed with Voltage-sensitive dyes. J. Comp. Neurol. 375, 89–108.

Kleinfeld, D., Mitra, P.P., Helmchen, F., Denk, W., 1998. Fluctuations and stimulus-induced changes in blood flow observed in individual capillaries in layers 2 through 4 of rat neocortex. Proc. Natl. Acad. Sci. 95 (26), 15741–15746.

Kong, Y., Zheng, Y., Johnston, D., Martindale, J., Jones, M., Billings, S., Mayhew, J., 2004. A model of the dynamic relationship between blood flow and volume changes during brain activation. J. Cereb. Blood Flow Metab. 24 (12), 1382–1392.

Krings, T., Erbericha, S.G., Roesslera, F., Reula, J., Throna, A., 1999. MR blood oxygenation level–dependent signal differences in parenchymal and large draining vessels: implications for functional MR imaging. Am. J. Neuroradiol. 20 (10), 1907–1914.

Lawson, C.L., Hanson, R.J., 1974. Solving Least Squares Problems. Prentice-Hall, p. 161. Chapter 23.

Li, P., Luo, Q., Luo, W., Chen, S., Cheng, H., Zeng, S., 2003. Spatiotemporal characteristics of cerebral blood volume changes in rat somatosensory cortex evoked by sciatic nerve stimulation and obtained by optical imaging. J. Biomed. Opt. 8 (4), 629–635.

Lou, H.C., Edvinsson, L., MacKenzie, E.T., 1987. The concept of coupling blood flow to brain function: revision required? Ann. Neurol. 22 (3), 289–297.

Lu, H., Patel, S., Luo, F., Li, S.J., Hillard, C.J., Ward, B.D., Hyde, J.S., 2004. Spatial correlations of laminar BOLD and CBV responses to rat whisker stimulation with neuronal activity localized by Fos expression. Magn. Reson. Med. 52 (5), 1060–1068.

Malonek, D., Grinvald, A., 1996. Interactions between electrical activity and cortical microcirculation revealed by imaging spectroscopy: implications for functional brain mapping. Science 272, 551–554.

Mandeville, J.B., Marota, J.J., Kosofsky, B.E., Keltner, J.R., Weissleder, R., Rosen, B.R., Weisskoff, R.M., 1998. Dynamic functional imaging of relative cerebral blood volume during rat forepaw stimulation. Magn. Reson. Med. 39 (4), 615–624.

Mandeville, J.B., Marota, J.J.A., Ayata, C., Zaharchuk, G., Moskowitz, M.A., Rosen, B.R., Weisskoff, R.M., 1999. Evidence of a cerebrovascular post-arteriole windkessel with delayed compliance. J. Cereb. Blood Flow Metab. 19 (6), 679–689.

Marota, J.J., Ayata, C., Moskowitz, M.A., Weisskoff, R.M., Rosen, B.R., Mandeville, J.B., 1999. Investigation of the early response to rat forepaw stimulation. Magn. Reson. Med. 41 (2), 247–252.

Masamoto, K., Kurachi, T., Takizawa, N., Kobayashi, H., Tanishita, K., 2003. Successive depth variations in microvascular distribution of rat somatosensory cortex. Brain Res. 995, 66–75.

Mayhew, J., Hu, D., Zheng, Y., Askew, S., Hou, Y., Berwick, J., Coffey, P.J., Brown, N., 1998. An evaluation of linear model analysis techniques for processing images of microcirculation activity. NeuroImage 7, 49–71.

Nemoto, M., Sheth, S., Guiou, M., Pouratian, N., Chen, J.W.Y., Toga, A.W., 2004. Functional signal- and paradigm-dependent linear relationships between synaptic activity and hemodynamic responses in rat somatosensory cortex. J. Neurosci. 24 (15), 3850–3861.

Ngai, A.C., Winn, H.R., 1995. Modulation of cerebral arteriolar diameter by intraluminal flow and pressure. Circ. Res. 77 (4), 832–840.

Ngai, A.C., Winn, H.R., 2002. Pial arteriole dilation during somatosensory stimulation is not mediated by an increase in CSF metabolites. Am. J. Physiol.: Heart Circ. Physiol. 282 (3), H902–H907.

Ohki, K., Chung, S., Ch'ng, Y.H., Kara, P., Reid, R.C., 2005. Functional imaging with cellular resolution reveals precise micro-architecture in visual cortex. Nature 433, 597–603.

Pain, F., Besret, L., Vaufrey, F., Grégoire, M., Pinot, L., Gervais, P., Ploux, L., Bloch, G., Mastrippolito, R., Lanièce, P., Hantraye, P., 2002. In vivo quantification of localized neuronal activation and inhibition in the rat brain using a dedicated high temporal-resolution β+-sensitive microprobe. Proc. Natl. Acad. Sci. 99 (16), 10807–10812.

Peppiatt, C.M., Howarth, C., Mobbs, P., Attwell, D., 2005. Regulation of capillary diameter in rat retina. J. Physiol. 568P, PC32.

Peppiatt, C.M., Howarth, C., Mobbs, P., Attwell, D., 2006. Bidirectional control of CNS capillary diameter by pericytes. Nature 443 (7112), 700–704.

Rodriguez-Baeza, A., Torre, F.R.-D.L., Ortega-Sanchez, M., Sahuquillo-Barris, J., 1998. Perivascular structures in corrosion casts of the human central nervous system: a confocal laser and scanning electron microscope study. Anat. Rec. 252 (2), 176–184.

Roy, C.W., Sherrington, C.S., 1890. On the regulation of the blood supply of the brain. J. Physiol. 11, 85–108.

Schulte, M.L., Wood, J.D., Hudetz, A.G., 2003. Cortical electrical stimulation alters erythrocyte perfusion pattern in the cerebral capillary network of the rat. Brain Res. 963 (1–2), 81–92.

Sheth, S.A., Nemoto, M., Guiou, M., Walker, M., Pouratian, N., Hageman, N., Toga, A.W., 2004. Columnar specificity of microvascular

oxygenation and volume responses: implications for functional brain mapping. J. Neurosci. 24 (3), 634–641.
Sheth, S.A., Nemoto, M., Guiou, M.W., Walker, M.A., Toga, A.W., 2005. Spatiotemporal evolution of functional hemodynamic changes and their relationship to neuronal activity. J. Cereb. Blood Flow Metab. 2pp. 1–12 (Mar).
Shibuki, K., Hishida, R., Murakami, H., Kudoh, M., Kawaguchi, T., Watanabe, M., Watanabe, S., Kouuchi, T., Tanaka, R., 2003. Dynamic imaging of somatosensory cortical activity in the rat visualized by flavoprotein autofluorescence. J. Physiol. 549 (3), 919–927.
Silva, A.C., Koretsky, A.P., 2002. Laminar specificity of functional MRI onset times during somatosensory stimulation in rat. Proc. Natl. Acad. Sci. 99 (23), 15182–15187.
Staiger, J.F., Zilles, K., Freund, T.F., 1996. Innervation of VIP-immunoreactive neurons by the ventroposteromedial thalamic nucleus in the barrel cortex of the rat. J. Comp. Neurol. 367 (2), 194–204.
Takano, T., Tian, G., Peng, W., Lou, N., Libionka, W., Han, X., Nedergaard, M., 2006. Astrocyte-mediated control of cerebral blood flow. Nat. Neurosci. 9, 260–267.
Toribatakea, Y., Tomita, K., Kawahara, N., Baba, H., Ohnari, H., Tanaka, S., 1997. Regulation of vasomotion of arterioles and capillaries in the cat spinal cord: role of actin and endothelin-1. Spinal Cord 35 (1), 26–32.
Turner, R., 2002. How much cortex can a vein drain? Downstream dilution of activation-related cerebral blood oxygenation changes. NeuroImage 16, 1062–1067.
Vanzetta, I., Hildesheim, R., Grinvald, A., 2005. Compartment-resolved imaging of activity-dependent dynamics of cortical blood volume and oximetry. J. Neurosci. 25 (9), 2233–2244.
Villringer, A., Them, A., Lindauer, U., Einhaupl, K., Dirnagl, U., 1994. Capillary perfusion of the rat brain cortex. An in vivo confocal microscopy study. Circ. Res. 75 (1), 55–62.
Vovenko, E., 1999. Distribution of oxygen tension on the surface of arterioles, capillaries and venules of brain cortex and in tissue in normoxia: an experimental study on rats. Pflugers Arch. 437 (4), 617–623.
Wang, X., Lou, N., Xu, Q., Tian, G., Peng, W.G., Han, X., Kang, J., Takano, T., Nedergaard, M., 2006. Astrocytic Ca2+ signaling evoked by sensory stimulation in vivo. Nat. Neurosci. 9 (6), 816–823.
Welsh, D.G., Segal, S.S., 1998. Endothelial and smooth muscle cell conduction in arterioles controlling blood flow. Am. J. Physiol.: Heart Circ. Physiol. 274 (1), H178–H186.
Woolsey, T.A., Rovainen, C.M., Cox, S.B., Henegar, M.H., Liang, G.E., Liu, D., Moskalenko, Y.E., Sui, J., Wei, L., 1996. Neuronal units linked to microvascular modules in cerebral cortex: response elements for imaging the brain. Cereb. Cortex 6 (5), 647–660.
Yacoub, E., Ugurbil, K., Harel, N., 2006. The spatial dependence of the poststimulus undershoot as revealed by high-resolution BOLD- and CBV-weighted fMRI. J. Cereb. Blood Flow Metab. 26 (5), 634–644.
Zhao, F., Wang, P., Hendrich, K., Ugurbil, K., Kim, S.-G., 2006. Cortical layer-dependent BOLD and CBV responses measured by spin-echo and gradient-echo fMRI: insights into hemodynamic regulation. NeuroImage 30 (4), 1149–1160.
Zheng, Y., Johnston, D., Berwick, J., Mayhew, J., 2001. Signal source separation in the analysis of neural activity in brain. NeuroImage 13 (3), 447–458.
Zheng, Y., Johnston, D., Berwick, J., Chen, D., Billings, S., Mayhew, J., 2005. A three-compartment model of the hemodynamic response and oxygen delivery to brain. NeuroImage 28 (4), 925–939.
Zonta, M., Angulo, M.C., Gobbo, S., Rosengarten, B., Hossmann, K.-A., Pozzan, T., Carmignoto, G., 2003. Neuron-to-astrocyte signaling is central to the dynamic control of brain microcirculation. Nat. Neurosci. 6 (1), 43–50.
Zwart, J.A.d., Silva, A.C., Gelderen, P.v., Kellman, P., Fukunaga, M., Chua, R., Koretsky, A.P., Frank, J.A., Duyn, J.H., 2005. Temporal dynamics of the BOLD fMRI impulse response. NeuroImage 24 (3), 667–677.